Toward the understanding of selective Si nano-oxidation by atomic scale simulations

Towards the Understanding of Selective Si Nano-oxidation by Atomic Scale Simulations

Umedjon Khalilov, Annemie Bogaerts and Erik C. Neyts

University of Antwerp, Department of Chemistry, research group PLASMANT, Universiteitsplein 1, 2610 Antwerp, Belgium

e-mail: umedjon.khalilov@uantwerpen.be

Conspectus

The continuous miniaturization of nanodevices, such as transistors, solar cells, and optical fibers, requires the controlled synthesis of (ultra)thin gate oxides (< 10 nm), including Si gate-oxide (SiO_2) with high quality at the atomic scale. Traditional thermal growth of SiO_2 on planar Si surfaces, however, does not allow to obtain such ultrathin oxide due to either the high oxygen diffusivity at high temperature or the very low sticking ability of incident oxygen at low temperature. Two recent techniques, both operative at low (room) temperature, have been put forward to overcome these obstacles: (i) hyperthermal oxidation of planar Si surfaces, and (ii) thermal or plasma-assisted oxidation of non-planar Si surfaces, including Si nanowires (SiNWs). These nano-oxidation processes are, however, often difficult to study experimentally, due to the key intermediate processes taking place on the nanosecond time scale.

In this Account, these Si nano-oxidation techniques are discussed from a computational point of view and compared to both hyperthermal and thermal oxidation experiments, as well as to well-known models of thermal oxidation, including the Deal-Grove, Cabrera-Mott, Kao

models and several alternative mechanisms. In our studies, we use reactive molecular dynamics (MD) and hybrid MD/Monte Carlo simulation techniques, applying the Reax force field. The incident energy of oxygen species is chosen in the range of 1-5 eV in *hyperthermal oxidation of planar Si surfaces* in order to prevent energy-induced damage. It turns out that hyperthermal growth allows for two growth modes, where the ultrathin oxide thickness depends either on (1) only the kinetic energy of the incident oxygen species at a growth temperature below T_{trans}=600 K, or (2) on both the incident energy and the growth temperature at a growth temperature above T_{trans}. These modes are specific to such ultrathin oxides, and are not observed in traditional thermal oxidation, nor theoretically considered by already existing models. In the case of *thermal or plasma-assisted oxidation of small Si nanowires*, on the other hand, the thickness of the ultrathin oxide is a function of the growth temperature and the nanowire diameter. Below T_{trans}, which varies with the nanowire diameter, partially oxidized SiNW are formed, whereas complete oxidation to a SiO_2 nanowire occurs only above T_{trans}. In both nano-oxidation processes at lower temperature ($T<T_{trans}$), final sandwich *c*-Si|SiO_x|*a*-SiO_2 structures are obtained due to a competition between overcoming the energy barrier to penetrate into Si subsurface layers and the compressive stress (~2-3 GPa) at the Si crystal/oxide interface. The overall atomic-simulation results strongly indicate that the thickness of the intermediate SiO_x ($x<2$) region is very limited (~0.5 nm) and constant irrespective of oxidation parameters. Thus, control over the ultrathin SiO_2 thickness with good quality is indeed possible by accurately tuning *the oxidant energy, oxidation temperature and surface curvature*.

In general, we discuss and put in perspective these two oxidation mechanisms for obtaining controllable ultrathin gate-oxide films, offering a new route towards the fabrication of nanodevices via selective nano-oxidation.

Introduction

Due to the continuous miniaturization of nanodevices, such as transistors, solar cells, and optical fibers, the controlled synthesis of (ultra)thin gate oxides is in high demand[1]. In particular, understanding how to control the Si gate-oxide (SiO_2) thickness with high quality at the atomic scale is very important. Unfortunately, traditional thermal growth of SiO_2 on a planar Si surface does not allow to obtain such high quality ultrathin oxide due to either the high oxygen diffusivity at high temperature or the very low sticking ability of incident oxygen at low temperature[2]. Two recent techniques, both operative at low (room) temperature, have been put forward to overcome these obstacles: (i) hyperthermal oxidation of planar Si surfaces[3-5], and (ii) thermal or plasma-assisted oxidation of non-planar Si surfaces[6-8]. These techniques are being intensively studied[9-12], in order to understand the oxidation process at the nanoscale. As a complicating factor, many of the key intermediate processes take place on the nanosecond time scale, which is often difficult to study experimentally. In this Account, these two selected Si nano-oxidation and subsequent ultrathin (< 2nm) SiO_2 formation processes are carefully studied by atomic-scale simulations and compared to both hyperthermal and thermal oxidation experiments, as well as to well-known models of thermal oxidation, including the Deal-Grove[13], Cabrera-Mott[14], Kao models[7] and several alternative mechanisms[15-18].

Hyperthermal oxidation of planar Si surfaces

Hyperthermal translational energy, in the range of about 1-500 eV, can activate a number of fundamental chemical processes in the near-surface region, including hyperthermal oxidation (HTO)[3]. Interestingly, tuning the incident energy in the hyperthermal range and selecting the projectile type can provide control over the oxidation process[4,5,9,10]. We study this process by applying ReaxFF-based molecular dynamics (MD) simulations[5,19].

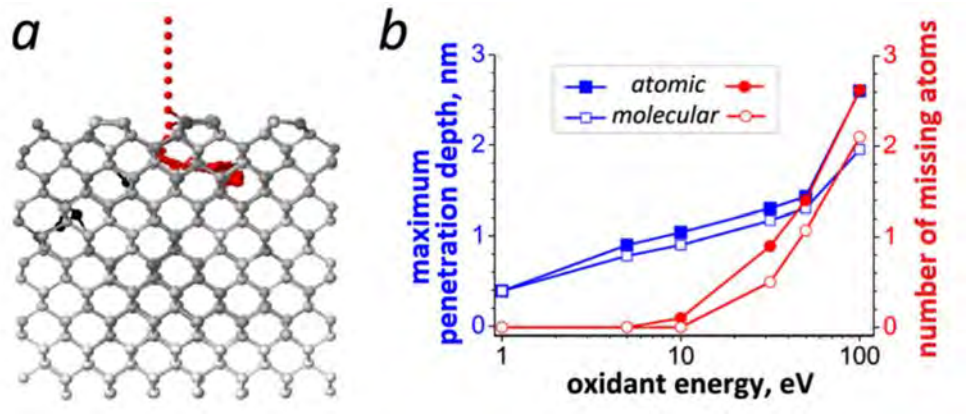

Figure 1 (*a*) Penetration trajectory and final position of O-atom (red) with an impact energy of 100 eV in the Si-crystal. The positions of the Si-atoms (black) are plotted once after collision, for the final configuration; the time interval between the consecutive positions of the impinging O-atom is 6.25 fs. (*b*) Maximum depth reached by the hyperthermal oxygen atoms (left y-axis, in blue color) after impact and calculated average number of missing atoms created in the Si-crystal per impact (right y-axis, in red color) as a function of impact energy for atomic and molecular oxygen impacts at near-room temperature. Courtesy of ref 19. Copyright 2011 ACS.

A typical example of such a simulation is shown in figure 1a, where a hyperthermal species is seen to penetrate deeper into the crystal. This is the direct result of their hyperthermal energy, as they can surmount the corresponding energy barriers, even at low temperatures[10,19]. In particular, O (or O_2) can penetrate in the Si(100)-{2x1} crystal with a size of 2.17 nm x 2.17 nm x 3.79 nm (figure 1a) to a depth of around 2 nm at an initial translation energy of 100 eV at 333 K[19]. While the interval between consecutive impacts is 3 ps, the projectiles typically already reach their maximum depth after 1 ps. Experimentally, room-temperature oxygen diffusion is a very slow process ($D \sim 10^{-20}$ cm^2/s)[20] and thus it is not taken into account in the simulations. Note that the maximum penetration depth is always smaller for molecule impacts than for atomic oxygen due to the immediate break-up upon O_2 collision (figure 1b). Since the molecules are given the same initial kinetic energy as the atoms, the individual atoms obtained after dissociation have less momentum and hence a lower velocity.

The penetrated oxygen can also induce damage or create a defect in the Si-crystal during the impact. The energy-dependent damage can be quantified by computing the average number of so-called *missing atoms* (MA) per impact[19]. Two distinct defect-generation mechanisms are observed for both atomic and molecular cases. In the first mechanism, an O with energy of 10 eV binds itself to two silicon atoms, forming a siloxane Si-O-Si bond. In this process, a Si-atom is pushed towards the surface, and is displaced from its equilibrium lattice location, creating a MA at that site. The second mechanism occurs through a simple knock-on displacement: an impinging O-atom with energy of more than 10 eV can displace a Si-atom from its lattice location due to a collision, thereby creating a vacancy-interstitial pair (a Frenkel pair). This is consistent with the experimental threshold energy window of 10-30 eV for the displacement of Si[21,22] and the Frenkel pair energy threshold for the [100] direction in Si (20 eV)[22]. The maximum energy that can be transferred to a Si-atom by an impinging O-atom, is given by $T_{max}=E_0(4m_{Si}m_O)/(m_{Si}+m_O)^2$, corresponding to about 92.5% of the initial impact energy. Therefore, secondary knock-on displacements can also occur if the initial impact energy is sufficiently high, due to Si-Si collision cascades in the bulk of the structure (figure 1a). Due to such energy-induced damage, the oxidant energy is preferentially in the range of 1-5 eV in order to perform damage-free HTO[4,5,9,10,23].

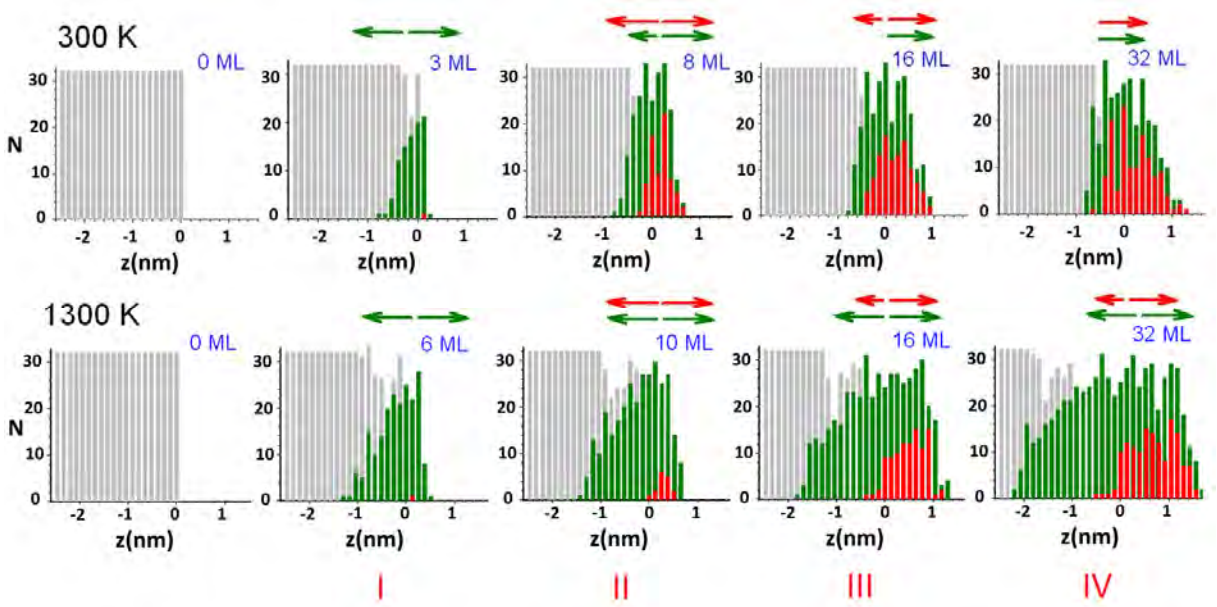

Figure 2 Oxide growth mechanisms in the case of hyperthermal oxidation at 300 K and 1300 K. Pure Si, intermediate SiO_x (x<2) and SiO_2 phases are represented by light grey, green and red bars, respectively. The average thickness of each Si (grey) layer is equal to 0.13 nm. Here, 1 monolayer (ML) equals 32 O-atoms. Courtesy of ref 22. Copyright 2012 ACS.

We can distinguish four stages in HTO process, both at low (300 K) and high (1300 K) temperature, as shown in figure 2. In stage I, the oxygen species with initial translational energy of 1-5 eV can surmount the energy barriers of the first and second Si subsurface layers, which are about 1.0 eV and 2.4 eV, respectively[4,5,9,10,18,19]. Indeed, the oxidant can easily be incorporated directly in the Si substrate even at (near-)room temperature[4,9,10]. This oxidation onset does not, however, correspond to the incubation period of thermal oxidation (TO)[16-18]. In the initial stage, the nonstoichiometric SiO_x layers grow simultaneously inward and outward (green arrows), normal to the surface at both temperatures. During the SiO_x oxide formation, the Si-suboxide Si^{i+} (i<4) components sequentially dominate in the consecutive $Si^{1+} \rightarrow Si^{2+} \rightarrow Si^{3+}$ conversion, corresponding to experimental observation[9], in which the Si consecutively binds to one, two and three nearest-neighbor O atoms.

In stage II, the inward growth rate of the oxidized layer drops significantly due to the activation energy barrier of the Si subsurface layers and the low diffusivity of the penetrated oxygen atoms at low temperature[17,20] (figure 2, 300 K). As a result, fast $Si^{1+} \rightarrow Si^{2+} \rightarrow Si^{3+} \rightarrow Si^{4+}$ conversion enhances the formation of new silica (SiO_2) layers in both directions (red arrows) and the thickness of the non-stoichiometric SiO_x region decreases drastically. Subsequently, the inward growth slows down considerably, namely for the SiO_x layers in stage III and for the SiO_2 layers in stage IV. The limit depth is nearly constant after the second stage and is found to be about 0.52 nm (0.39 nm) and 0.91nm (0.78 nm) for atomic (molecular) oxidation with kinetic energies of 1 and 5 eV, respectively[23].

At high temperature (above 500 K), however, interstitial oxygen species are sufficiently mobile to surmount the activation energy barrier and thus both the inward and outward growth of the SiO_x and the SiO_2 regions continues in all stages. Consequently, the concentration of the suboxide species drastically increases relative to the Si^{4+} species with increasing growth temperature[23], resulting in a broad SiO_x region, which is also observed in TO experiments[24]. Particularly, the number of the Si^{1+} species dominates in the non-stoichiometric region due to the increasing diffusivity of the oxygen atoms above 500 K. Such temperature-dependent oxidation behavior is also experimentally observed, i.e., interstitial neutral O and O_2 become mobile above 200°C (~ 500 K) and 400°C (~ 700 K), respectively[25].

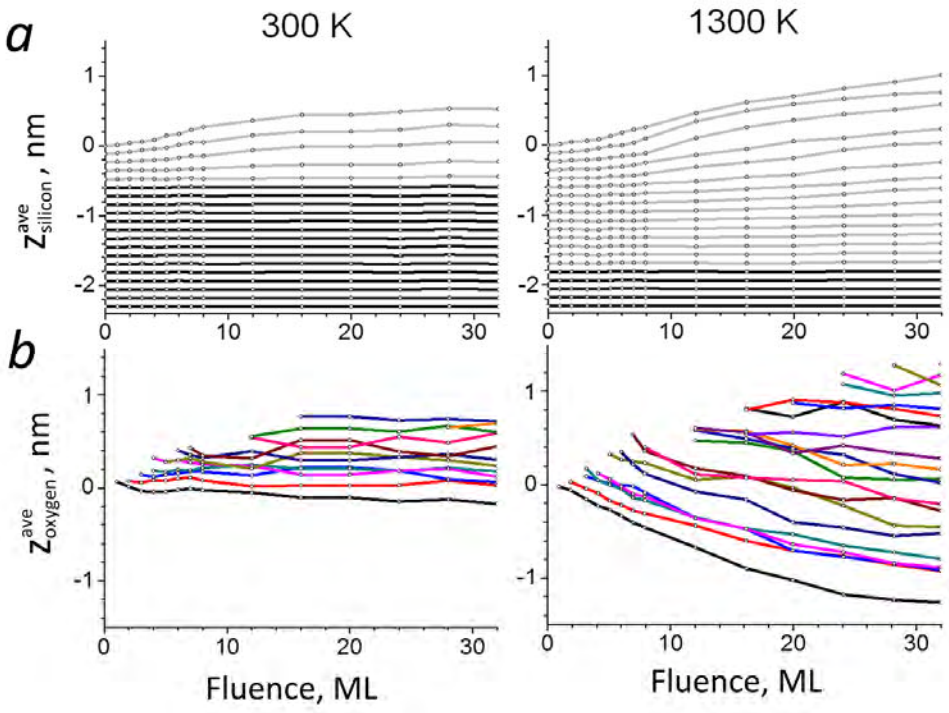

Figure 3 Evolution of (*a*) the growth of oxygenated Si (grey) on Si-crystal (black layers), as shown by the average z-coordinate of the silicon atoms per line (corresponds to 32 Si-atoms), and (*b*) the inward diffusion depth of penetrated oxygen (z-coordinate of each penetrated 32 O-atoms is averaged and lines are represented in different colors in sake of clarity) during HTO by oxygen atoms of 5 eV, at temperatures of 300 K and 1300 K, respectively. Here, z = 0 Å corresponds to the top-most layer of the original pristine Si lattice. Courtesy of ref 22. Copyright 2012 ACS.

Analysis of the outward and inward displacement of silicon and oxygen species in the oxide growth process also allows a deeper understanding of the growth mechanism, by comparing with suggested mechanisms for thermal Si oxidation[13-15]. In the initial stage, the upper surface and subsurface Si layers remain in place, while some oxygen atoms penetrate up to the limit depth at low temperature (figure 3a). Afterwards, the top layers gradually expand and the distance between the layers eventually equals the thickness of one oxide layer (0.26 nm)[9]. According to the "reactive layer" model[15,18] and the Cabrera-Mott mechanism[14], silicon atoms diffuse (upwards) through the thin reactive layer and react with oxygen at the top of this layer, forming the SiO_2 phase. The atomistic simulations, however, point out that there is no

outward displacement of single silicon atoms and therefore these models do not properly describe the growth behavior in HTO.

At low temperature, hyperthermal oxygen atoms cross the $SiO_2|SiO_x$ interface by virtue of their kinetic energy, react with Si^{i+} (i<4) atoms and reach their maximum depth in the non-stoichiometric SiO_x region[26]. The inward oxygen growth (figure 3b) is nearly inhibited by the associated energy barrier and thus the oxidation rate of new Si layers can be a slow process, similar to TO, occurring on a time scale of 10^3 to 10^5 s depending on the experimental conditions at 300 K[17,20]. Thus, the kinetic energy of the incident oxygen atoms is the dominant factor in low temperature oxidation. In contrast, above 600 K, mobile O or O_2 can penetrate/diffuse down to the $SiO_x|Si$ interface and react with the Si-crystal[26]. We call this temperature the transition temperature T_{trans}. Interestingly, the oxidation mechanism resembles thermal wet and dry oxidation, which is described by the Deal-Grove model[13]. In this model, the oxygen reacts with the Si-crystal after diffusing through the oxide layers. However, this model and its extensions[16,17] fail to describe the oxidation kinetics of ultrathin (< 4 nm) films[2] in HTO in two situations: (*a*) there is no pre-existing oxide layer on the Si surface prior to oxidation; and (*b*) suitable parameters are needed to describe direct oxidation. The latter is also not taken into account in the Cabrera-Mott mechanism, in which a field in the Si oxide is created due to upward electron transport, which is held responsible for the oxygen (ion) inward migration[14].

Based on the above, we conclude that hyperthermal growth allows for two growth modes[23], which are not observed nor expected in TO of planar Si surfaces:

(i) When the temperature is below T_{trans} (i.e., $T < T_{trans}$), the oxide thickness depends only on the kinetic energy of the incident oxygen species;

(ii) When $T > T_{trans}$, the oxide thickness depends on both the incident energy and the growth temperature.

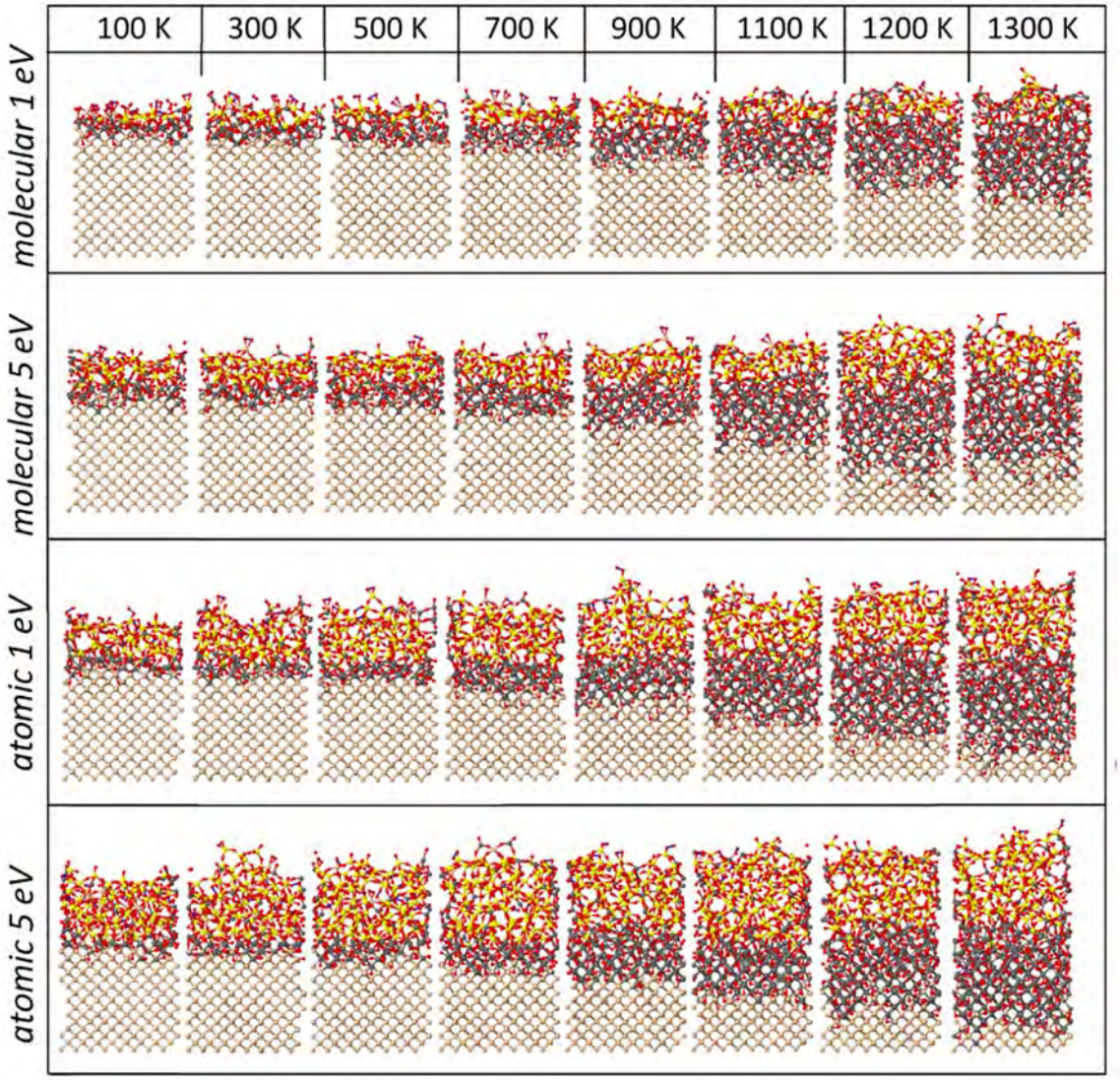

Figure 4 HTO of silicon after 32 ML of O-atoms in atomic and molecular impacts with energy of 1-5 eV. Here, the Si, SiO_x, SiO_2 phases and oxygen atoms are colored light grey, dark grey, yellow and red, respectively. Courtesy of ref 22. Copyright 2012 ACS.

Besides the effect of the growth temperature and the incident kinetic energy, the change of the oxide thickness is also caused by the type of oxygen species[23] (figure 4). Due to lower momentum after their dissociation, the sticking probability of molecules is always smaller than the sticking probability of atoms[5,26]. Consequently, oxygen molecules do not penetrate as

deep in the surface as the oxygen atoms, resulting in a thinner thickness at the same conditions[4,5,9].

However, a relatively rough interface is obtained in molecular oxidation compared to atomic oxidation above T_{trans}, indicating that the roughness increases with decreasing oxide thickness. At room temperature, the roughness of the SiO_x interface increases from 0.1 nm to constant values of about 0.15 nm and 0.21 nm for atomic and molecular oxidation by 5 eV particles, respectively[27]. While the second value is somewhat larger, both values are quite close to experimental interfacial roughness values ranging from 0.15 to 0.2 nm in HTO at room temperature[4]. Such a change in roughness can be attributed to the competition between energy barriers in Si layers and compressive stresses at the silicon/oxide interface[28]. Because of such stresses, some Si-epoxide (denoted SiØSi) linkages[29,30] appear at the interface as well, which can be regarded as an intermediate state of the Si-O-Si→SiØSi→Si-Si transition[27]. Indeed, oxygen atoms in the SiO_x region can be pushed towards the SiO_2 oxide region at low temperature[27]. Since the stress decreases with increasing growth temperature[7], low-temperature oxidation (~2 GPa at 300 K)[28] reduces the oxygen diffusivity in the interface significantly and thus the ultrathin oxide can be grown and tuned at temperatures below T_{trans}[27].

In *Table 1*, the final thickness of the interface and the silica region is given as a function of the kinetic energy and type of oxidant at 300 K. Prior to attaining the final thickness, the SiO_x thickness increases in the direct oxidation stage for both species, but it decreases again up to about 0.5 nm in the slow oxidation stage, which is in agreement with experimental thickness ranges from 0.15 to 1 nm[4,10].

Table 1. Final thickness of the oxygenated silicon, split up into transition and silica regions, for both atomic and molecular impacts at three different energies at room temperature.

Incident oxygen species	incident energy, eV	thickness of oxygenated silicon, nm		
		SiO_x	SiO_2	*Total*
Atom	1.0	0.55	1.52	2.07
	3.0	0.56	1.69	2.25
	5.0	0.58	1.87	2.45
Molecule	1.0	0.48	0.52	1.0
	3.0	0.52	0.63	1.15
	5.0	0.56	0.91	1.47

Note that the final value of the silica thickness is 0.63 nm in the case of O_2 with 3 eV, which is very close to the experimental result of 0.6 nm at the same conditions[9]. Also, the obtained total oxide thickness is 2.45 nm in 5 eV atomic oxidation with a fluence of 1.22×10^{17} O atoms·cm^{-2}, which is in fair agreement with the experimental oxide thickness of about 2.9 nm obtained using a fluence of 8×10^{17} O atoms·cm^{-2} of 4.6 eV at 297 K, as determined from experimental measurements[4]. In general, the table shows that the average total thickness of the saturated oxide layer obtained by O is about twice the value obtained for O_2. This clearly indicates the possibility to control the oxide layer thickness by the choice of the impinging species and the impact energy below T_{trans}.

Given that thickness control is possible, a structural analysis of the obtained oxide is important as well. In figure 5, the calculated radial distribution function (RDF) shows that the Si-O (α peak), O-O (β peak) and Si-Si (γ peak) bonds are distributed around 0.16 nm, 0.25 nm and 0.32 nm, respectively, in agreement with both experimental values and other MD calculations[31-33], indicating that the obtained silica structure is amorphous (*a*-SiO_2). However,

at low temperature, some unexpected O-O non-bonded neighbors (β_2 peak) are found with a distance of 0.226 nm, close to the β peak, caused by the interfacial stress.

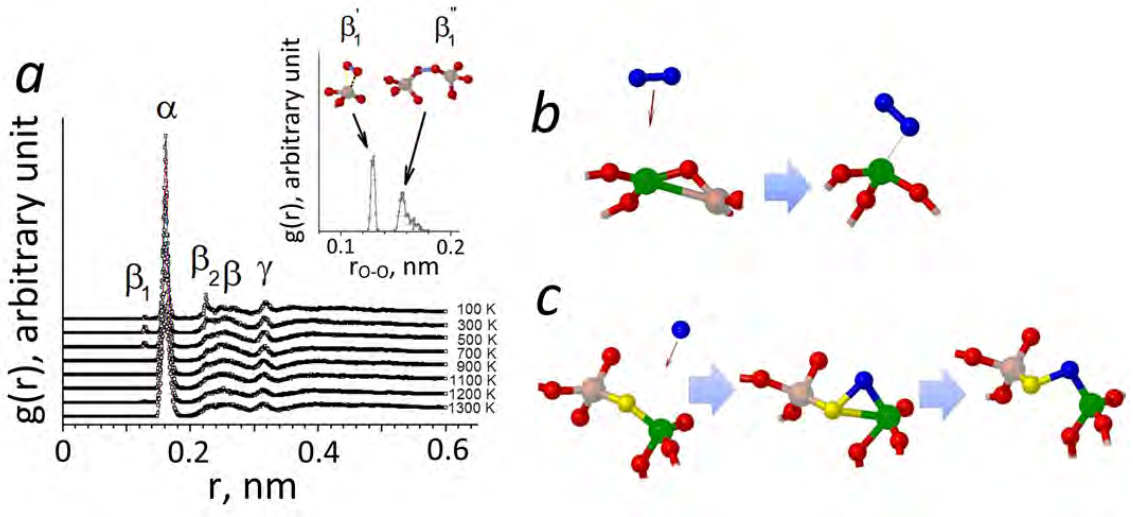

Figure 5 (*a*) Total radial distribution functions of the SiO_2 structure during HTO for 3 eV atomic impacts at different temperatures, and the partial distribution function for the O-O distance at 300 K. (b) and (c) Two types of oxygen peroxyl bridge bonds in silica and their formation mechanisms. Reacting Si and O atoms in the initial structures are colored in green and yellow, respectively, while the incident particles are colored blue. Courtesy of refs 22 (*a*) and 25 (*b*,*c*). Copyright 2012 and 2013 ACS.

Also, some small peaks indicate the presence of two kinds of peroxyl bridges with distances of around 0.13 nm and 0.16 nm (β_1' and β_1'' in figure 5a), which can be formed following two mechanisms. In the first mechanism (figure 5b), the incident molecule reacts with a Si-epoxide structure near the interface and binds weakly with the Si^{3+}, thereby creating an oxygen defect. In the second mechanism (figure 5c), the incident atom reacts with Si^{4+} atoms and creates oxygen peroxyl bonds in *a*-SiO_2. As a result, two SiO_2 molecules connect through the peroxyl bond, creating a Si deficiency in this region. The first defect is found to be stable (E_a = -1.093 eV) with respect to the second defect (E_a = 1.017 eV). Both disappear above T_{trans}, indicating that the number of peroxyl bridges significantly decreases with increasing

growth temperature[23]. The existence of such bridges and three-fold bond configurations in *a*-SiO_2 was already reported experimentally[9,14,25] and theoretically[17,34].

In the oxide structure, the O-Si-O angles are distributed at around 110° in both the atomic and molecular oxidation cases, corresponding to the tetrahedral silicon angle (109.5°). Also, two Si-O-Si angle distributions were found, i.e., at around 150° and 160° for the molecular and atomic oxygen cases, respectively. Both values are fairly close to the experimental value (i.e., 151°±11°) of the Si-O-Si angle in vitreous (amorphous) silica[31,32].

The calculated mass density (2250 kg/m^3) of the SiO_2 structure is very close to the value for amorphous silica[32].

Thermal or plasma-assisted oxidation of small-diameter Si nanowires

From our calculations, we also predict the possible formation of ultrathin *a*-SiO_2 oxide with a tunable thickness by thermal or plasma-assisted oxidation of Si nanowires (SiNWs)[8,35]. Note that although plasma exposure of solid (metal) surfaces leads to the formation of different nanostructures[36], we only focus on the layer-type SiO_2 formation. Figure 6 presents simulation results, showing the TO process of small SiNWs with a diameter of 2 nm using O_2 molecules with thermal energies corresponding to either low (300 K) or high (1273 K) temperature. Every 10 ps, a new molecule is included in the gas-phase with a random direction and is initially positioned at least 1 nm far from any system atom/molecule. Simulations are performed by reactive MD and hybrid MD/Monte-Carlo (MD/tfMC) techniques in the case of thermal and plasma-assisted SiNW oxidations, respectively[5, 35, 37]. In these calculations, 1 ML corresponds to 56 O-atoms.

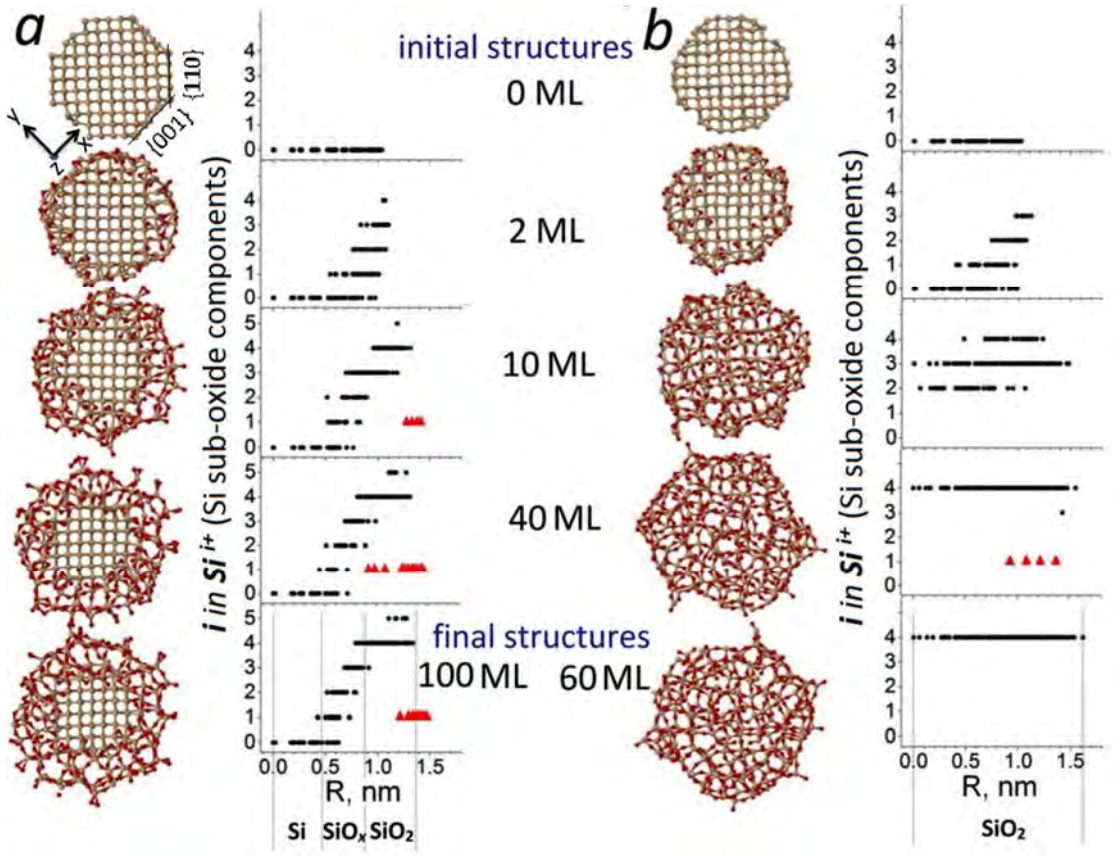

Figure 6 Oxide formation and growth as a function of the O_2 fluence in the 2 nm SiNW (cross-section) at (*a*) 300 K and (*b*) 1200 K. Each structure is analyzed by the radial distribution of the Si-(sub)oxide components (black circles) and the O-O peroxyl bridges (red triangles). R is the radial distance from the center of the SiNW to the nanowire atoms in the (x,y) plane. Courtesy of ref 36. Copyright 2013 RSC.

At 1200 K, the SiNW is completely oxidized after 10 ML of O_2 fluence, in agreement with the experimental observation that this is a sufficient temperature for complete oxidation of a SiNW with an initial radius of 15 nm or less[12]. At 300 K, however, the oxide growth process saturates after 40 ML, resulting in an oxide thickness of 1 nm. The Si-core radius drops from 1 to 0.5 nm, and consequently, the total SiNW radius increases to about 1.5 nm. Since the molecular volume of Si-oxide is larger than the atomic volume of Si, the newly formed oxide exerts a tensile stress, in order to accommodate the volume expansion[7,11,12]. At the end of the oxidation process, the distribution of the Si-suboxide components in the oxidized SiNW

indicates two different final structures, i.e., silicon-silica ($Si|SiO_x|SiO_2$) and pure silica (SiO_2), which are obtained at low and high temperatures, respectively. The calculated mass density of both oxide structures is around 2250 kg/m^3, which is close to the value for amorphous silica[31,32].

The RDF analysis shows three peaks, i.e., Si-O bond, non-bonded O-O and Si-Si neighbor distances, distributed around 0.16, 0.25 and 0.32 nm, respectively. This is in agreement with both experiments and with other calculations[31-33], and indicates that the oxide is *a*-SiO_2. In the oxide structure, the distribution of O-Si-O and Si-O-Si angles fluctuates around 150° and 110°, respectively, also indicating that the structure is amorphous[31-33]. At low temperature, two extra RDF peaks at 0.23 nm and 0.38 nm indicate the Si-Si first and second nearest-neighbors in the Si-core (*c*-Si), respectively. Also, the average Si-Si-Si angle is about 110° in the Si-core. Moreover, an additional O-Si-O angle is found at around 30° due to peroxyl bonds (0.13 nm)[34], which also play a role in the appearance of over-coordinated Si^{5+} species (see β_1' in figure 5) on the *a*-SiO_2 surface.

Indeed, we can obtain *c*-$Si|SiO_x|$*a*-SiO_2 structures at low temperature, whereas a *c*-Si nanowire completely converts to an *a*-SiO_2 nanowire at high temperature. Note that this conversion/transition may also depend on the physical state of the nano-system due to the Gibbs-Tomson effect[38]. The formation of such partially-oxidized SiNW structure due to self-limiting oxidation[11,12], can be theoretically explained by the Kao model[7], which is a popular extension of the traditional Deal-Grove model for wet (H_2O) oxidation of non-planar (convex and concave) Si surfaces with μm-length. However, the kinetics of the early-oxidation stage in dry (O_2) and plasma-assisted (O, HO, HO_2, etc.) oxidation cannot properly be described by this model[8,35,39]. Also, this microscale model fails for the nanoscale regime, in which stresses depend also on the crystallographic facets of the (ultra)small SiNW[36,40].

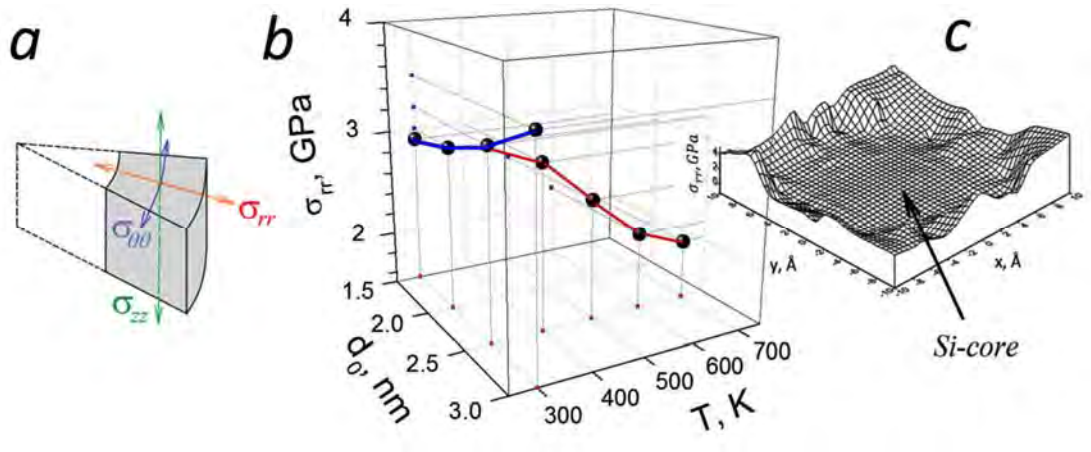

Figure 7 (a) Initial stresses in a SiNW; (b) averaged radial σ_{rr} stresses in the *c*-Si|*a*-SiO_2 interface of the final oxidized SiNW structure as a function of the diameter (or curvature) and oxide growth temperature; (c) the interfacial σ_{rr} stress in the x-y plane for oxidized Si-NW (with initial diameter d_0=3 nm) grown at 300 K: the (0, 0) position corresponds to the SiNW center. Courtesy of ref 36. Copyright 2013 RSC.

The calculations show that while the axial (σ_{zz}) stress is nearly zero, the radial (σ_{rr}) and shear ($\sigma_{\theta\theta}$) stresses (figure 7a) depend on the non-oxidized nanowire facet at low temperatures (figure 6a). For instance, σ_{rr} is tensile (negative) for the {110} facet, while it is compressive (positive) for the {001} facet of small Si-NWs (d_0=1.5 - 3 nm) at 300 K[8,37]. Also the sticking probability of oxidant species depends on such facet-dependent stresses in the oxidation onset[37]. In the oxidation, on the one hand, compressive radial stresses at the *c*-Si|*a*-SiO_2 interface (figure 7c) continuously slow down the reaction rate, while the compressive pressure (i.e., $p = -\frac{1}{2}(\sigma_{rr} + \sigma_{\theta\theta})$) in *a*-$SiO_2$ can, on the other hand, reduce the oxidant diffusion and solubility, resulting in self-limiting oxidation, similar to micro-scale SiNW oxidation[7,11,12].

Indeed, the inward oxide growth depends on the σ_{rr} rather than $\sigma_{\theta\theta}$ and σ_{zz} stresses in the Si-core. During the oxidation, the compressive radial stress gradually increases with values of 1.6 GPa, 2.0 GPa and 3.0 GPa after 10 ML, 40 ML and 60 ML, respectively, at 300 K. At still higher fluence, the interfacial stress remains constant at about 3 GPa. The overall results show

that the final interfacial stresses inversely depend on growth temperature (i.e., $\sigma_{rr} \sim 1/T$)[40]. For instance, the stresses are 3.2 GPa, 3.0 GPa, 2.6 GPa, 2.2 GPa, and 2.04 GPa at 300 K, 400 K, 500 K, 600 K and 700 K, respectively for the 2.5 nm Si-NW(figure 7b). This is in excellent agreement with the micro-scale oxidation theory[7]. However, curvature-dependent behavior of the interfacial stresses is not accounted for in this theory. Indeed, we find averaged interfacial stresses of 2.9 GPa, 3.0 GPa, 3.2 GPa, and 3.5 GPa for the NWs with 1.5 nm, 2 nm, 2.5 nm and 3 nm diameter, respectively (figure 7b). This curvature-stress phenomenon can be explained by considering that the sub-10 nm Si-core deforms more to compensate for the volume expansion of the surface oxide layer, resulting in a smaller compressive stress[40]. Furthermore, crystal orientation effects may play a role as well in this nanoscale phenomenon[37].

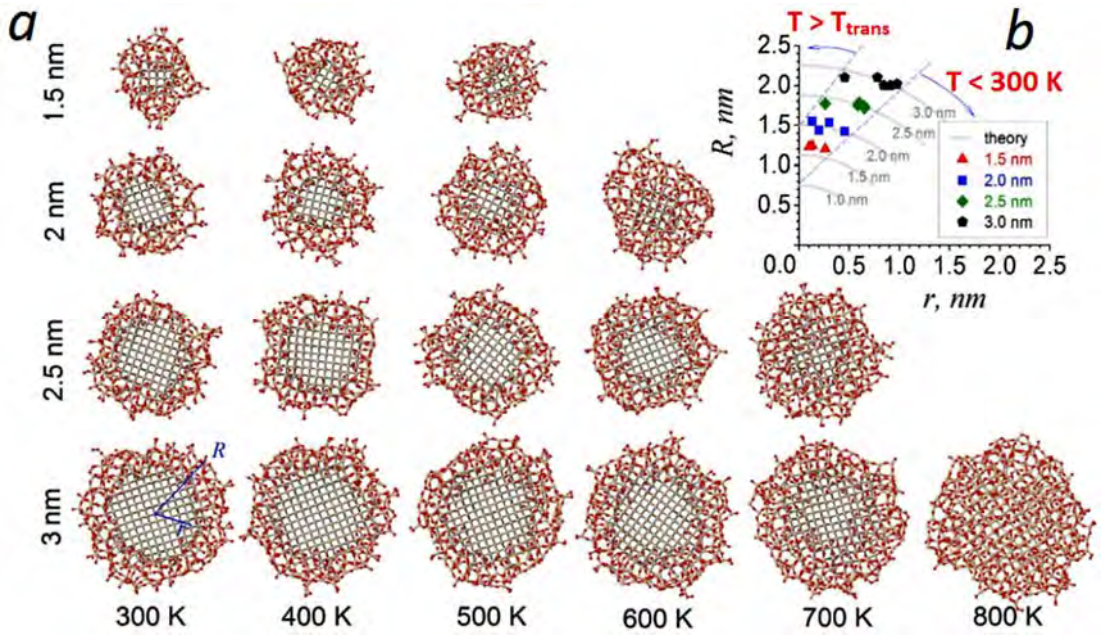

Figure 8 (*a*) Cross-sections of the *c*-Si|SiO_x|*a*-SiO_2 nanowires with initial diameter in the range 1.5 – 3 nm after oxidation at T=300-800 K. (*b*) Final radii of Si-core (*r*) and SiNW (*R*), compared with theoretical calculations, derived from *equation (1)*. Courtesy of ref 36. Copyright 2013 RSC.

Thanks to such temperature and curvature dependent stresses, control over the ultrathin oxide seems possible. Figure 8a demonstrates that both the Si-core radius (*r*) and the SiNW radius

(R) depend on the initial diameter (d_0) and inversely depend on the oxidation temperature (T), i.e., $r\ (or\ R) \sim \frac{d_0}{T}$. The maximum radius of the Si-core reaches about 0.26 nm, 0.46 nm, 0.65 nm and 0.91 nm for 1.5, 2, 2.5 and 3 nm diameter Si-NWs, respectively. Due to the increasing diffusivity and mobility of the penetrated oxygen atoms[37], the core radius drops with rising temperature and consequently the nanowire converts to a pure SiO_x ($x \leq 2$) nanowire at a certain T_{trans}, which is roughly equal to 500 K, 600 K, 700 K and 800 K for Si-NWs with diameters of 1.5 nm, 2 nm, 2.5 nm and 3 nm, respectively.

Note that, however, the contribution of long timescale diffusion[17,20] is not fully accounted for in these MD simulations and thus the partially oxidized structure might finally become fully oxidized even below T_{trans}. Nevertheless, the final radii of the *c*-Si|SiO_x|*a*-SiO_2 nanowires, as obtained by the simulations, can be compared with the following volume balance, to which also experimental results are often compared[12]:

$$\pi(R^2 - r^2)L - \pi(R_0^2 - r_0^2)L = \frac{\Omega_{SiO_2}}{\Omega_{Si}}\pi(r_0^2 - r^2)L \quad (1)$$

where r_0, r and R_0, R are the initial and final radii of Si-core and oxidized SiNW, respectively; L is the SiNW length; Ω_{SiO2} is the molecular volume of SiO_2 (0.045 nm^3) and Ω_{Si} is the atomic volume of Si (0.02 nm^3)[7]. Based on the initial conditions (i.e., r_0=R_0), the relation between the final SiNW (R) and Si-core (r) radii for partially oxidized structures with initial diameters (d_0=$2r_0$) is calculated by $R = \sqrt{2.25r_0^2 - 1.25r^2}$, which is derived from eq. (1). The obtained results are very close to this theoretical calculation (grey curves in figure 8b), clearly indicating that the nanowire diameter (or curvature) and growth temperature are the main parameters to control the growth of nanowires with ultrathin oxide[37].

In addition to thickness control, low-temperature thermal[8] and plasma-assisted oxidation[35] also hold promise to obtain ultra-small SiNWs with diameters less than 1 nm by etching (or removing) their oxide shell, which in turn allows obtaining nanowires with larger band gaps[6].

Conclusions

In this Account, two Si nano-oxidation techniques as options to control the ultrathin Si-oxide thickness are discussed from a computational point of view. To prevent energy-induced damage, the incident energy of oxygen species is preferentially chosen in the range of 1-5 eV in *hyperthermal oxidation of planar Si surfaces*. The hyperthermal growth mechanism shows two growth modes, which are not observed in the traditional thermal oxidation, nor theoretically considered by already existing models. In these modes, the oxide thickness depends either on (1) the kinetic energy of the incident oxygen species if the growth temperature is below the transition temperature (T_{trans}=600 K), or (2) on both the incident energy and the growth temperature if the growth temperature is above T_{trans}. Below T_{trans}, the oxygen mobility (diffusivity) is significantly reduced due to interfacial stresses in the SiO_x region, allowing to control the thickness of ultrathin *a*-SiO_2. Alternatively, control over such ultrathin amorphous oxide can also be obtained by *thermal or plasma-assisted oxidation of small Si nanowires*. In the self-limiting oxidation at low temperature, partially oxidized nanostructures are obtained due to curvature and temperature dependent stresses at the *c*-Si|*a*-SiO_2 interface. In both oxidation cases, the type of oxygen species and their fluence (or flux) can affect the oxide thickness as well, besides the energy and temperature effects. The obtained oxide structure is amorphous, whereas the structure contains some intrinsic defects, such as O peroxyl linkages and Si-epoxide bonds, which are also observed in thermal oxidation experiments.

In general, these two Si nano-oxidation methods strongly indicate that the scaling of the ultrathin thickness is possible by accurately tuning *the oxidant energy*, *the growth temperature* and *the surface curvature*.

Biographical Information

Umedjon Khalilov was born in Uzbekistan, 1977. He obtained his PhD in Chemistry from the University of Antwerp in 2013 with a dissertation titled “New perspectives on thermal and hyperthermal oxidation of Si surfaces”. The work was done in collaboration with the Interuniversity Microelectronics Centre (IMEC), Belgium. He is currently working as a post-doctoral researcher at the same university.

Annemie Bogaerts was born in Belgium, 1971. She obtained her PhD in chemistry in 1996 from the University of Antwerp. She is full professor at the University of Antwerp since 2012, and head of the interdisciplinary research group PLASMANT. Her research focuses on studying various types of plasmas for environmental, medical and material science applications, both by modeling and experiments. She has written around 360 peer-reviewed publications since 1995, including 14 invited reviews, as well as 11 invited book chapters. She is also editor of the journal "Spectrochimica Acta: Part B", where she is responsible for the review papers. She is in the editorial board of several journals, and she was many times guest editor of special issues.

Erik C. Neyts was born in Belgium, 1977. In 2006, he obtained his PhD from the University of Antwerp, where he currently is associate professor in Chemistry. His field of research is the simulation and modeling of nanostructures and dynamical processes at the nanoscale. He has (co-)authored over 100 peer-reviewed journal papers, a book chapter on invitation, as well as several high-impact reviews. Moreover, he served as guest-editor of special issues in J. Phys. D: Appl. Phys. and in Catal. Today, in which nanostructure growth takes a prominent place.

References

1. International Technology Roadmap for Semiconductors 2015 edition, May 21, 2015 (http://www.itrs2.net/).

2. Gusev, E. P.; Lu, H. C.; Gustafsson, T.; Garfunkel, E. Growth mechanism of thin silicon oxide film on Si(100) studied by medium-energy ion scattering. *Phys. Rev. B*, **1995**, *52*, 1759-1775.

3. Jacobs, D. C. Reactive Collisions of Hyperthermal Energy Molecular Ions with Solid Surfaces. *Annu. Rev. Phys. Chem.,* **2002**, 53, 379–407.

4. Tagawa, M.; Yokota, K.; Ohmae, N.; Kinoshita, H.; Umeno, M. Oxidation Properties of Hydrogen-Terminated Si(001) Surfaces Following Use of a Hyperthermal Broad Atomic Oxygen Beam at Low Temperatures. *Jpn. J. Appl. Phys., Part 1*, **2001**, 40, 6152.

5. Khalilov, U.; Neyts, E. C.; Pourtois, G.; van Duin, A. C. T. Can We Control the Thickness of Ultrathin Silica Layers by Hyperthermal Silicon Oxidation at Room Temperature? *J. Phys. Chem. C,* **2011**, 115, 24839–24848.

6. Ma, D. D. D.; Lee, C. S.; Au, F. C. K.; Tong, S. Y.; Lee, S. T. Small-Diameter Silicon Nanowire Surfaces. *Science*, **2003**, 299, 1874.

7. Kao, D.–B.; McVittie, J. P.; Nix, W. D.; Saraswat, C. K. Two-Dimensional Thermal oxidation of Silicon - II.Modeling Stress Effects in Wet Oxides. *IEEE Tran. Elec. Dev.*, **1988**, 35, 25-37.

8. Khalilov, U.; Pourtois, G.; van Duin, A. C. T.; Neyts, E. C. Self-Limiting Oxidation in Small-Diameter Si Nanowires *Chem. Mater.,* **2012**, 24, 2141–2147.

9. Yoshigoe, A.; Teraoka, Y. Time resolved photoemission spectroscopy on Si(001)-2x1 surface during oxidation controlled by translational kinetic energy of O_2 at room temperature. *Surf. Sci.* **2003**, 532-535, 690-697.

10. Kisa, M.; Minton, T. K.; Yang, J. C. Structural comparison of SiO_x and SiO_x formed by the exposure of silicon (100) to molecular oxygen and to hyperthermal atomic oxygen. *J. Appl. Phys.*, **2005**, 97, 023520.

11. Liu, H. I.; Biegelsen, D. K.; Johnson, N. M.; Ponce, F. A.; Pease, R. F.W. Self-limiting oxidation of Si nanowires. *J. Vac. Sci. Technol.* B, **1993**, 11, 2532.

12. Büttner, C. C.; Zacharias, M. Retarded oxidation of Si nanowires. *Appl. Phys. Lett.*, **2006**, 89, 263106.

13. Deal, B. E.; Grove, A. S. General Relationship for the Thermal Oxidation of Silicon. *J. Appl. Phys.*, **1965**, 36, 3770–3778.

14. Atkinson, A. Transport processes during the growth of oxide films at elevated temperature. *Rev. Mod. Phys.*, **1985**, 57, 437-470.

15. Stoneham, A. M.; Grovenor, C. R. M.; Carezzo, A. Oxidation and the structure of the silicon/oxide interface. *Philos. Mag. B*, **1987**, 55, 201-10.

16. Massoud, H. Z.; Plummer, J. D.; Irene, E. A. Thermal Oxidation of Silicon in Dry Oxygen. *J. Electrochem. Soc.*, **1985**, 132, 1745.

17. Cerofolini, G. F.; Mascolo, D.; Vlad, M. O. A model for oxidation kinetics in air at room temperature of hydrogen-terminated (100) Si. *J. Appl. Phys.*, **2006**, 100, 054308.

18. Kageshima, H.; Shiraishi, K. First-Principles Study of Oxide Growth on Si(100) Surfaces and at SiO_2/Si(100) Interfaces. *Phys. Rev. Lett.,* **1998**, 81, 5936-5939.

19. Neyts, E. C.; Khalilov, U.; Pourtois, G.; van Duin, A. C. T. Hyperthermal Oxygen Interacting with Silicon Surfaces Adsorption, Implantation, and Damage Creation. *J. Phys. Chem. C,* **2011**, 115, 4818–4823.

20. Jiang, Z.; Brown, R. A. Atomistic Calculation of Oxygen Diffusivity in Crystalline Silicon. *Phys. Rev. Lett.*, **1995**, 74, 2046.

21. Rabalais, J. W. *Low Energy Ion-Surface Interactions*, Wiley, Chester, 1994; p 610.

22. Holmström, E.; Kuronen, A.; Nordlund, K. Threshold defect production in silicon determined by density functional theory molecular dynamics simulations. *Phys. Rev. B*, **2008**, *78*, 045202.

23. Khalilov, U.; Pourtois, G.; van Duin, A. C. T.; Neyts, E. C. Hyperthermal Oxidation of Si(100)2x1 Surfaces: Effect of Growth Temperature. *J. Phys. Chem. C,* **2012**, 116, 8649–8656.

24. Dumpala, S.; Broderick, S. R.; Khalilov, U.; Neyts, E. C.; van Duin, A. C. T.; Provine, J.; Howe R. T.; Rajan, K. Integrated atomistic chemical imaging and reactive force field molecular dynamic simulations on silicon oxidation. *Appl. Phys. Lett.,* **2015**, 106, 011602.

25. Kajihara, K.; Miura, T.; Kamioka, H.; Aiba, A.; Uramoto, M.; Morimoto, Y.; Hirano, M.; Skuja, L.; Hosono, H. Diffusion and reactions of interstitial oxygen species in amorphous SiO_2: A review. *J. Non-Cryst. Solids*, **2008**, 354, 224-232.

26. Khalilov, U.; Pourtois, G.; Huygh, S.; van Duin, A. C. T.; Neyts, E. C.; Bogaerts, A. New Mechanism for Oxidation of Native Silicon Oxide. *J. Phys. Chem. C,* **2013**, 117, 9819–9825.

27. Khalilov, U.; Pourtois, G.; van Duin, A. C. T.; Neyts, E. C. On the *c*-Si|*a*-SiO_2 Interface in Hyperthermal Si oxidation at Room Temperature. *J. Phys. Chem. C,* **2012**, 116, 21856–21863.

28. Donnadieu, P.; Blanquet, E.; Jakse, N.; Mur, P. Detection of subnanometric layer at the Si|SiO_2 interface and related strain measurements. *Appl. Phys. Lett.*, **2004**, 85, 5574.

29. Stefanov, B. B.; Gurevich, A. B.; Weldon, M. K.; Raghavachari, K.; Chabal, Y. J. Silicon Epoxide: Unexpected Intermediate during Silicon Oxide Formation. *Phys. Rev. Lett.*, **1998**, 81, 3908-3911.

30.Schoeters, B.; Neyts, E. C.; Khalilov, U.; Pourtois G.; Partoens, B. Stability of Si Epoxide Defects in Si nanowires: A Mixed Reactive Force Field/DFT Study. *Phys. Chem. Chem. Phys.*, **2013**, 15, 15091-15097.

31. Da Silva, J.; Pinatti, D.; Anderson, C.; Rudee, M. A refinement of the structure of vitreous silica. *Philos. Mag.*, **1975**, 31, 713.

32. Brückner, R. Properties and structure of vitreous silica, I, *Journal of Non-Crystalline Solids* **1970**, 5, 123-175.

33. Fogarty, J. C.; Aktulga, H. M.; Grama, A. Y.; van Duin, A. C. T.; Pandit, S. A reactive molecular dynamics simulation of the silica-water interface. *J. Chem. Phys.*, **2010**, 132, 174704.

34. Stoneham, A. M.; Szymanski, M. A.; Shluger, A. L. Atomic and ionic processes of silicon oxidation. *Phys. Rev. B*, **2001**, 63, 221304-07.

35. Khalilov, U.; Yusupov, M.; Bogaerts A.; Neyts, E. C. Selective Plasma Oxidation of Ultrasmall Si Nanowires. *J. Phys. Chem. C,* **2016**, 120, 472–477.

36. Xu, S.; Huang, S. Y.; Levchenko, I.; Zhou, H. P.; Wei, D. Y.; Xiao, S. Q.; Xu, L. X.; Yan, W. S. and Ostrikov, K. Highly Efficient Silicon Nanoarray Solar Cells by a Single-Step Plasma-Based Process. *Adv. Energy Mater*., **2011**, 1, 373-376.

37. Khalilov, U.; Pourtois, G.; Bogaerts, A.; van Duin, A. C. T.; Neyts, E. C. Reactive Molecular Dynamics simulations on SiO_2-coated ultra-small Si-nanowires. *Nanoscale,* **2013**, 5, 719-725.

38. Buffat, Ph. & Borel, J-P. Size effect on the melting temperature of gold particles. *Phys. Rev. A* **1976**, 13, 2287-2298.

39. Levchenko, I.; Cvelbar U.; Ostrikov, K. Kinetics of the initial stage of silicon surface oxidation: Deal-Grove or surface nucleation? *Appl. Phys. Lett*., **2009**, 95, 021502.

40. Kim, B. -H.; Pamungkas, M. A.; Park, M.; Kim, G.; Lee, K. -R.; Chung, Y. -C. Stress evolution during the oxidation of silicon nanowires in the sub-10 nm diameter regime. *Appl. Phys. Lett.*, **2011**, 99, 143115.

Conspectus image